*magnetism*

MDPI

*Article*

# Effect of the Non-Magnetic Ion Doping on the Magnetic Behavior of $MgCr_2O_4$

**Fuxi Zhou [1,2,3,†], Zheng He [2,3,†], Donger Cheng [2,3,4,5], Han Ge [6], Wenjing Zhang [7], Xiao Wang [2,3], Pengfei Zhou [2,3], Wanju Luo [2,3], Zhengdong Fu [7], Xinzhi Liu [4,5], Liusuo Wu [6,8], Lunhua He [3,9], Yanchun Zhao [1,10,*] and Erxi Feng [2,3,*]**

1 Key Laboratory of Advanced Processing and Recycling of Nonferrous Metals, School of Materials Science and Engineering, Lanzhou University of Technology, Lanzhou 730050, China; zhoufx@ihep.ac.cn
2 Institute of High Energy Physics, Chinese Academy of Sciences (CAS), Beijing 100049, China; hezheng@ihep.ac.cn (Z.H.); chengder@mail2.sysu.edu.cn (D.C.); xiaowang@ihep.ac.cn (X.W.); zhoupf@ihep.ac.cn (P.Z.); luowj@ihep.ac.cn (W.L.)
3 Spallation Neutron Source Science Center, Dongguan 523803, China; lhhe@ihep.ac.cn
4 Guangdong Provincial Key Laboratory of Magnetoelectric Physics and Devices, School of Physics, Sun Yat-sen University, Guangzhou 510275, China; liuxzh39@mail.sysu.edu.cn
5 Centre for Physical Mechanics and Biophysics, and Centre for Neutron Science and Technology, School of Physics, Sun Yat-sen University, Guangzhou 510275, China
6 Department of Physics, Southern University of Science and Technology, Shenzhen 518055, China; geh5@sustech.edu.cn (H.G.); wuls@sustech.edu.cn (L.W.)
7 Neutron Science Center, Songshan Lake Materials Laboratory, Dongguan 523808, China; wjzhangd2022@hust.edu.cn (W.Z.); fuzhendong@sslab.org.cn (Z.F.)
8 Shenzhen Key Laboratory of Advanced Quantum Functional Materials and Devices, Southern University of Science and Technology, Shenzhen 518055, China
9 Beijing National Laboratory for Condensed Matter Physics, Institute of Physics, Chinese Academy of Sciences, Beijing 100190, China
10 Wenzhou Pump and Valve Engineering Research Institute, Lanzhou University of Technology, Wenzhou 325105, China
* Correspondence: zhaoyanchun@lut.edu.cn (Y.Z.); fengex@ihep.ac.cn (E.F.)
† These authors contributed equally to this work.

check for updates

Academic Editor: Andrea Atrei

Received: 3 July 2025
Revised: 13 August 2025
Accepted: 20 August 2025
Published: 25 August 2025

**Citation:** Zhou, F.; He, Z.; Cheng, D.; Ge, H.; Zhang, W.; Wang, X.; Zhou, P.; Luo, W.; Fu, Z.; Liu, X.; et al. Effect of the Non-Magnetic Ion Doping on the Magnetic Behavior of $MgCr_2O_4$. *Magnetism* **2025**, *5*, 19. https://doi.org/10.3390/magnetism5030019

**Correction Statement:** This article has been republished with a minor change. The change does not affect the scientific content of the article and further details are available within the backmatter of the website version of this article.

**Copyright:** © 2025 by the authors. Licensee MDPI, Basel, Switzerland. This article is an open access article distributed under the terms and conditions of the Creative Commons Attribution (CC BY) license (https://creativecommons.org/licenses/by/4.0/).

## Abstract

Geometrically frustrated magnets exhibit exotic excitations due to competing interactions between spins. The spinel compound $MgCr_2O_4$, a three-dimensional Heisenberg antiferromagnet, hosts both spin-wave and spin-resonance modes, but the origin of its resonant excitations remains debated. Suppressing magnetic order via non-magnetic doping can help isolate these modes in neutron scattering studies. We synthesized $Ga^{3+}$ and $Cd^{2+}$-doped $MgCr_2O_4$ via solid-state reaction and analyzed their structure and magnetism. $Ga^{3+}$ doping (0–20%) causes anomalous lattice shrinkage due to site disorder from $Ga^{3+}$ occupying both $Mg^{2+}$ and $Cr^{3+}$ sites. Magnetically, $Ga^{3+}$ doping drives the system from the antiferromagnetic order to a spin-glass state, fully suppressing magnetic ordering at 20% doping. In contrast, $Cd^{2+}$ replaces only $Mg^{2+}$, expanding the lattice and meantime inducing strong spin-glass behavior. At 10% $Cd^{2+}$, long-range antiferromagnetic order is entirely suppressed. Thus, 10% Cd-doped $MgCr_2O_4$ offers an ideal platform to study the resonant magnetic excitations without any spin-wave interference.

**Keywords:** $MgCr_2O_4$; geometric frustration magnets; doping; antiferromagnetic order

## 1. Introduction

Magnetic frustration emanating from competing exchange interactions at the microscopic scale engenders macroscopic degeneracy of spin configurations and exotic magnetic

excitations [1,2]. Predominantly, such phenomena manifest in materials known as geometrically frustrated magnets, wherein magnetic ions occupy the vertices of specific lattices. Examples include $YbMgGaO_4$ [3], which features a triangular lattice of $Yb^{3+}$ ions and exhibits a quantum spin liquid state with itinerant excitations and quantum spin fluctuations. $ZnCu_3(OH)_6Cl_2$ [4,5], which hosts a spin-1/2 kagome lattice of $Cu^{2+}$ ions and whose ground state may lie near a quantum critical point or resemble a critical spin liquid, exhibits highly diffusive scattering intensity in neutron scattering experiments, as reported by Tian-Heng Han et al. [6], distinct from that of non-frustrated quantum magnets and indicative of strong quantum fluctuations—providing direct evidence of its frustrated antiferromagnetic nature. Neutron diffuse scattering measurements on the kagome lattice compound $Y_{0.5}Ca_{0.5}BaCo_4O_7$ reveal the presence of only a short-range chiral order, without the emergence of long-range antiferromagnetic ordering, making it a compelling realization of a frustrated antiferromagnet [7]. In addition, neutron scattering experiments on this system reveal the onset of spin-freezing at low temperatures, accompanied by a broad dynamic response with significant temperature dependence [8]. Additionally, $Na_4Ir_3O_8$ [9] is present, a three-dimensional frustrated magnet with a hyperkagome lattice of $Ir^{4+}$, whose ground state has been proposed as a rare 3D realization of a spin liquid. The pyrochlore lattice, another archetype of 3D geometry-frustrated lattice, has garnered enormous attention for decades as it could present a plethora of unique quantum behaviors, including spin ice, magnetic monopoles, quantum spin liquids, and spin resonances [10–13]. The lattice structure of magnetic ions is the motif of a 3D network of corner-sharing tetrahedra and is identified in two main categories of natural materials: pyrochlore oxides $A_2B_2O_7$ [12,14–16] with dual pyrochlore lattices on both A and B atomic sites and spinel chalcogenides $AB_2X_4$ (X = O, S, Se) [17–23], where only the B-site cations form a pyrochlore lattice.

The magnesium trinary compound $MgCr_2O_4$, as a member of chromium-based spinel oxides $ACr_2O_4$ (A = Zn, Mg, Cd, Hg) [19,24–29], is considered as a classical Heisenberg pyrochlore antiferromagnet. The sole magnetic ion $Cr^{3+}$ ($3d^3$, $S = 3/2$) in $MgCr_2O_4$ [25], with half-filled $t_{2g}$ orbitals and quenched orbital momentum, resides on a pyrochlore lattice and is antiferromagnetically coupled with its six nearest $Cr^{3+}$ neighbors. The Curie–Weiss temperature $\theta_{CW}$ of $MgCr_2O_4$ varies from $-346$ to $-430$ K [25,26,30], indicating strong antiferromagnetic interactions among $Cr^{3+}$, and an apparent hump around 50 K in the magnetic susceptibility provides evidence of short-range spin ordering. Upon cooling well below $|\theta_{CW}|$, $MgCr_2O_4$ undergoes intricate phase transitions with antiferromagnetic transition temperatures $T_N$ ranging from 12 to 16 K [25,31,32] and a concomitant decrease in lattice symmetry from cubic (space group: $Fd\bar{3}m$) to tetragonal phase (space group: $I4_1/amd$). The large value of $f = |\theta_{CW}|/T_N > 20$ clearly indicates that the whole spin system in $MgCr_2O_4$ is highly frustrated. Neutron powder diffraction (NPD) experiments have shown multiple magnetic propagation vectors within the antiferromagnetic phase of $MgCr_2O_4$ below $T_N$ [24,26,31]. Notably, these wave vectors exhibit various combinations across different NPD experiments, yet the magnetic moment of $Cr^{3+}$ remains unsaturated and consistently smaller than the fully ordered moment of $Cr^{3+}$ (3.87 $\mu_B$) in most instances. Below the Néel temperature, magnetic Bragg reflections are indexed by multiple propagation vectors, including $k_{L,1}$ = (1/2, 1/2, 0) and $k_{L,2}$ = (1, 0, 1/2) [26,31], associated with a partially resolved "L phase" [26,31,33]. In addition, some samples exhibit a distinct "H phase" above $T_N$ but below $T_H \approx 16$ K, characterized by a propagation vector $k_H$ = (0, 0, 1) [26,32]. Some reports of $k = (1/2, 1/2, 1/2)$ [24] further emphasize the complexity of the system's magnetic ordering and suggest the coexistence of multiple magnetic phases. Additionally, sharp and non-dispersive spin resonances at energy transfer $E = 4.5$, 9.0, 13.5... meV observed in inelastic neutron scattering (INS) spectra were interpreted as transitions between two quantum levels of spin clusters, leading to the classification

of $MgCr_2O_4$ as a potential molecular spin liquid [24,31,34]. However, this hypothesis has recently been contested from a classical perspective, and the debate surrounding its magnetic ground state remains unresolved [33,34].

Chemical doping is usually considered a promising method to understand complicated magnetic orders and underlying spin–lattice couplings in $MgCr_2O_4$, particularly by modulating its low-temperature antiferromagnetic behaviors [29,35–37]. Differences in ionic radius ratios and volatilization rates among different elements often hinder the formation of a pure phase, making detailed synthesis and doping studies essential. Moreover, understanding how doping affects the magnetic ion sites is crucial for identifying appropriate doping levels that can effectively suppress magnetic ordering. According to the report in (S. E. Dutton, PRB, 2011) [25], the magnetic properties of $MgCr_2O_4$ are profoundly sensitive to metal atoms' nonstoichiometry both at $Mg^{2+}$ and $Cr^{3+}$ sites, and even minor alterations in the microscopic chemical environment significantly impact its Néel temperature $T_N$ and spin correlations above $T_N$. A similar effect is also observed in its homologous compound, $ZnCr_2O_4$ [35–39], where $Cd^{2+}$ substitution for $Mg^{2+}$ and $Ga^{3+}$ substitution for $Cr^{3+}$ effectively suppress its $T_N$. To our knowledge, there has been no systematic investigation of chemical doping in magnesium spinel oxide $MgCr_2O_4$.

In this work, we report the effects of $Ga^{3+}$ and $Cd^{2+}$ doping on the crystal structure and magnetic properties of $MgCr_2O_4$. $Ga^{3+}$ doping effectively modulates the magnetic properties of the $MgCr_2O_4$ system by weakening its antiferromagnetic (AFM) order, inducing a transition to a spin-glass state, and eventually driving the system into a paramagnetic state at higher doping levels. Similarly, the introduction of $Cd^{2+}$ also suppresses AFM interactions. However, due to the larger ionic radius of $Cd^{2+}$ and the resulting stronger lattice distortion, this effect is more sensitive, enabling spin-freezing to occur at relatively low doping concentrations and temperatures.

## 2. Materials and Methods

The spinel chromium oxides $Mg(Cr_{1-x}Ga_x)_2O_4$ ($x$ = 0, 0.05, 0.10, 0.15, and 0.20) and $Mg_{1-x}Cd_xCr_2O_4$ ($x$ = 0, 0.05, 0.10, 0.15, and 0.20) were synthesized via a conventional high-temperature solid-state reaction method [37,38]. Based on the X-ray powder diffraction (XRD) refinement results, we found that a 1% reduction in the $Cr_2O_3$ (99.99%, Shanghai Aladdin Biochemical Technology Co., Ltd., Shanghai, China) stoichiometric amount was necessary to obtain a pure phase. $Mg(Cr_{1-x}Ga_x)_2O_4$ was prepared by mixing stoichiometric amounts of $Cr_2O_3$, $Ga_2O_3$ (99.99%, Shanghai Aladdin Biochemical Technology Co., Ltd., Shanghai, China), and MgO (99.99%, Shanghai Aladdin Biochemical Technology Co., Ltd., Shanghai, China) in air, with a 1% reduction in $Cr_2O_3$. The mixture was pre-sintered at 800 °C for 12 h in air. After cooling, it was reground and subsequently reacted at 1200 °C for 24 h to obtain $Mg(Cr_{1-x}Ga_x)_2O_4$($x$ = 0, 0.05, 0.10, 0.15, and 0.20). Similarly, MgO, $Cr_2O_3$, and CdO (99.99%, Shanghai Aladdin Biochemical Technology Co., Ltd., Shanghai, China) were mixed in stoichiometric ratios and subjected to the same synthesis procedure to obtain $Mg_{1-x}Cd_xCr_2O_4$($x$ = 0, 0.05, 0.10, 0.15, and 0.20).

The crystallographic structures of the samples were characterized at room temperature using XRD (Rigaku Smartlab 3kW, Rigaku Corporation, Tokyo, Japan) with Cu K$\alpha$ radiation ($\lambda$ = 1.54 Å). The DC magnetic susceptibilities of all samples were measured using the Physical Property Measurement System (PPMS) from Quantum Design (San Diego, CA, USA), under the condition of zero-field cooling (ZFC) and field cooling (FC) processes. The time-of-flight neutron powder diffraction (NPD) measurements were conducted on $Mg(Cr_{1-x}Ga_x)_2O_4$ ($x = 0.20$) samples using the General Purpose Powder Diffractometer (GPPD) at China Spallation Neutron Source (CSNS), and the diffraction data were refined by using the Rietveld method with FullProf (Version: January-2021).

## 3. Results and Discussions

### *3.1. $MgCr_2O_4$ Doped with Ga*

To elucidate the structural modifications induced by Ga doping in the spinel compound $MgCr_2O_4$, a combination of X-ray and neutron diffraction analysis was employed. The phases and the cation site occupancy were carefully determined. Figure 1b shows the X-ray diffraction patterns of $Mg(Cr_{1-x}Ga_x)_2O_4$ ($x = 0$, 0.05, 0.10, 0.15, and 0.20) measured at room temperature over the $2\theta$ range of 10°–80°. All diffraction peaks can be indexed to the cubic spinel structure with space group $Fd\bar{3}m$ (No. 227), and no impurity phases were observed in any of the synthesized samples. A representative Rietveld refinement profile for the undoped $MgCr_2O_4$ sample is shown in Figure 1c. Initial XRD refinements with the model of Ga substitution only on Cr (B-site) yielded poor agreement, implying possible Ga on the A-site. However, due to the poor sensitivity of the light elements, such as Mg, XRD is not able to determine the ratio of Mg/Ga on the A-site. Thus, the neutron powder diffraction and refinement were employed because of the strong contrast of the neutron coherent scattering length of Mg (5.375 fm), Ga (7.288 fm), and Cr (3.635 fm) element [40]. The typical *tof*-NPD refinement for the sample Mg $(Cr_{1-x}Ga_x)_2O_4$, $x = 0.20$, is presented in Figure 1d, indicating that the actual composition is $(Mg_{0.754}Ga_{0.246})(Cr_{0.923}Ga_{0.077})_2O_4$. This demonstrates that $Ga^{3+}$ ions substitute on both the A-site ($Mg^{2+}$) and B-site ($Cr^{3+}$), resulting in a complex compound with the nominal formula $(Mg_{1-x}Ga_x)(Cr_{1-y}Ga_y)_2O_4$ while preserving the spinel structure. The site disorder between $Mg^{2+}$ and $Ga^{3+}$ ions has been also observed in other compounds, such as the the nonmagnetic layers in $YbMgGaO_4$ [3].

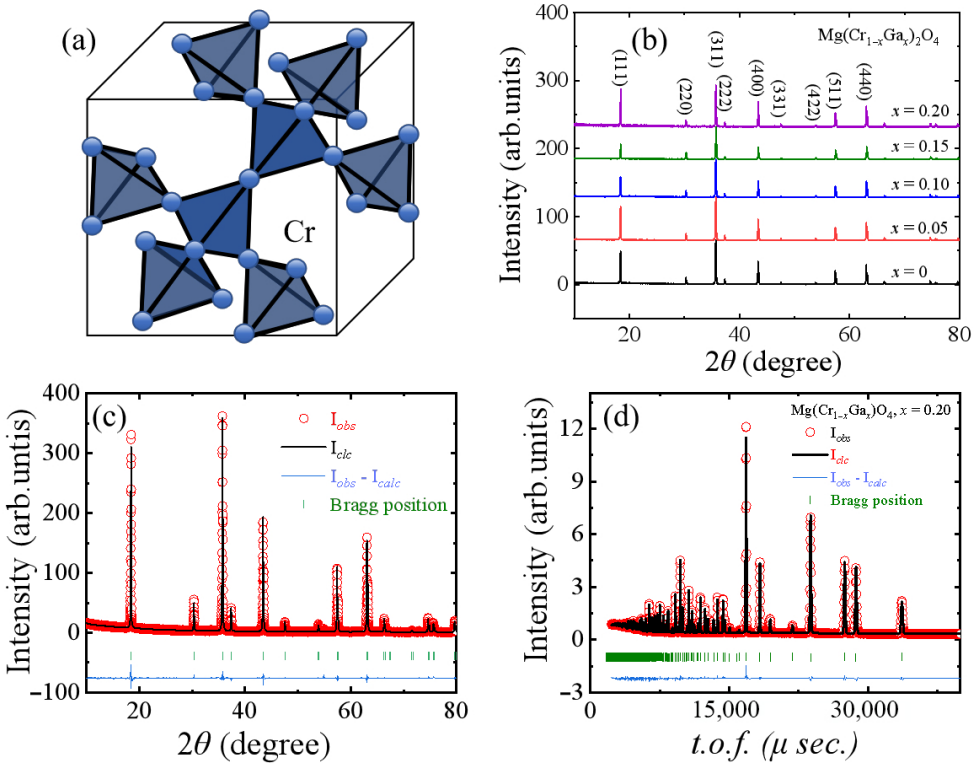



**Figure 1.** (**a**) The crystal structure of the $MgCr_2O_4$ compound; (**b**) the XRD patterns of the samples $Mg(Cr_{1-x}Ga_x)_2O_4$ ($x$ = 0, 0.05, 0.10, 0.15, and 0.20); the combined Rietveld refinement of (**c**) XRD and (**d**) NPD of the sample $Mg(Cr_{1-x}Ga_x)_2O_4$ ($x$ = 0.20), The Wyckoff positions of the atoms are in Table A1 of the Appendix A.

The obtained crystallographic parameters mainly from the XRD Rietveld refinement of the Gd-doped sample $MgCr_2O_4$ are presented in Figure 2. As shown in Figure 2a,b, with the increases in the named $Ga^{3+}$ doping amount, both $Cr^{3+}$ and $Mg^{2+}$ occupancies of the

A-site and B-site decrease. While the Cr occupancy nearly remains unchanged, the Mg occupancy increases drastically as the total doping amount of the Ga is constant. The above result suggests Ga ions prefer to stay at the A-site in the low doping level. Although $Ga^{3+}$ doping does not change the overall symmetry of the spinel structure, the lattice constant *a* slightly decreases with Ga doping increasing due to the smaller ionic radius of $Ga^{3+}$. A monotonic decrease in the Cr–Cr and Mg–Mg bond lengths is also observed, consistent with the decrease in lattice constant [Figure 2d,e]. Furthermore, Figure 2f shows that the decrease in the weighted average ionic radius at the A-site outweighs the slight increase at the B-site, suggesting that lattice shrinkage is primarily driven by substitution at the A-site. Such lattice contraction arises from the distinct size mismatch between dopant and host cations: $Ga^{3+}$ in octahedral coordination (B-site) has a slightly larger ionic radius (62 pm) than $Cr^{3+}$ (61.5 pm), while $Ga^{3+}$ in tetrahedral coordination (A-site) is substantially smaller (47 pm) than $Mg^{2+}$ (57 pm). In previously reported studies on Ga-doped $ZnCr_2O_4$ [25,37], no evidence of Ga incorporation at the A-site was observed, which may be attributed to the large ionic radius mismatch between $Zn^{2+}$ (60 pm) and $Ga^{3+}$ (47 pm) [41], resulting in an unfavorable substitution environment.

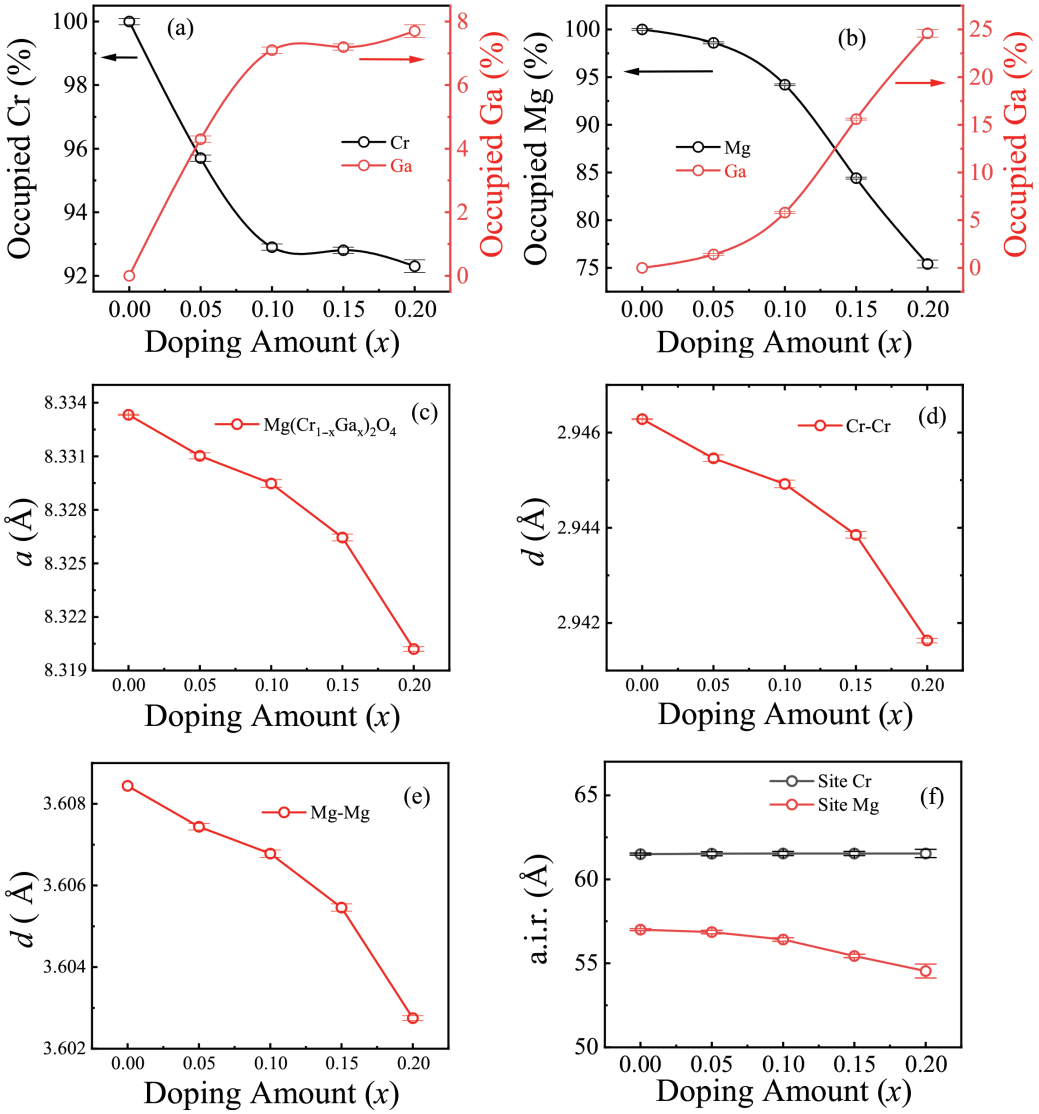



**Figure 2.** The occupancy of Ga at the $Cr^{3+}$ and $Mg^{2+}$ sites is presented in (**a**,**b**); the variations of the lattice constants for all $Mg(Cr_{1-x}Ga_x)_2O_4$ samples (**c**); (**d**,**e**) the changes in the Cr-Cr and Mg-Mg bond lengths, respectively; (**f**) the changes in the average ionic radii (a.i.r.) after Ga incorporation at the $Cr^{3+}$ and $Mg^{2+}$ sites. Detailed data can be found in Table A2 of the Appendix A.

Figure 3 presents the temperature-dependent DC magnetic susceptibility, $\chi(T)$, of $Mg(Cr_{1-x}Ga_x)_2O_4$ ($x = 0$, 0.05, 0.10, 0.15, and 0.20) measured under zero-field-cooled (ZFC) and field-cooled (FC) conditions with an applied magnetic field of 0.2 T in the temperature range 2.0–300 K. The Néel temperature ($T_N$) is determined by the drop temperature in $\chi(T)$. For the undoped sample ($x = 0$), $\chi(T)$ drops sharply at 12.6 K, indicating the antiferromagnetic ordering as reported [24,42]. With increasing Ga doping, $T_N$ gradually shifts toward lower temperatures and falls below 2.0 K for $x = 0.20$ (see Figure 4a), which is out of the measurable temperature range on a conventional PPMS. Further magnetic susceptibility measurement of this sample with He3 or Dilution refrigerator equipment is needed to clarify the possible antiferromagnetic order at extreme low temperature. Unlike the $T_N$ of $MgCr_2O_4$ increase with the lattice constants' decrease under pressure [43], our results of Ga-doping reveal contrary behavior. One possibility is that the incorporation of $Ga^{3+}$ ions partially replaces the magnetic $Cr^{3+}$ ions, resulting in magnetic site dilution. This weakens the magnetic interactions and ultimately leads to a reduction in the $T_N$ value.

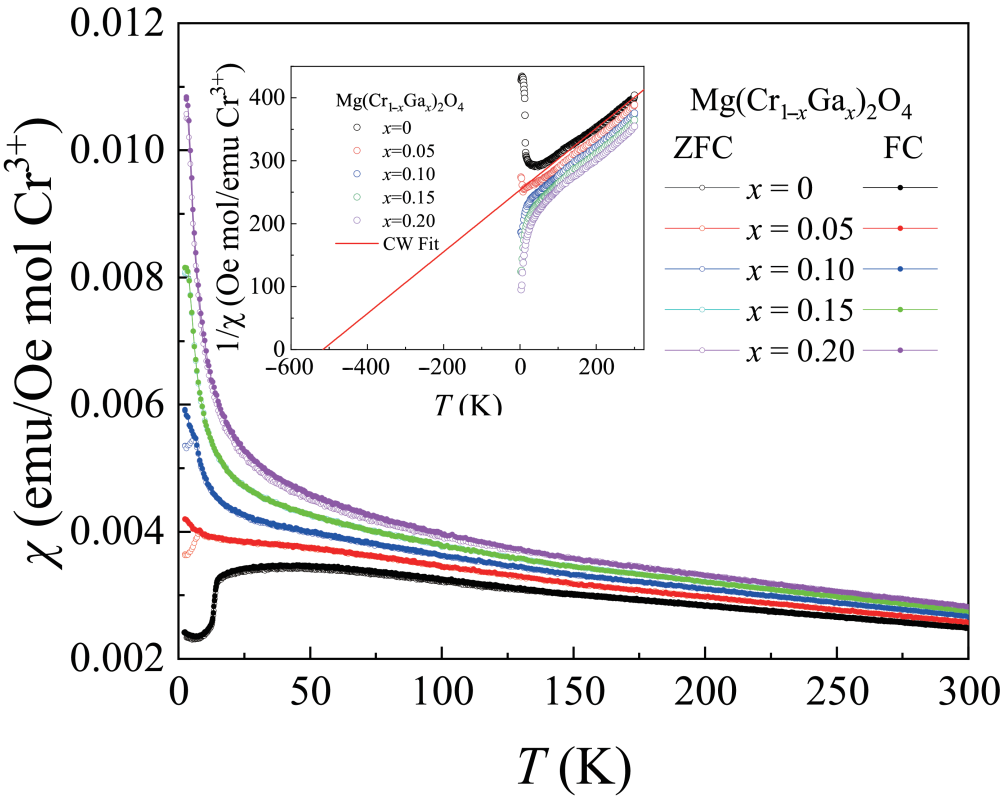



**Figure 3.** Temperature dependence of the DC magnetic susceptibilities $\chi(T)$ for $Mg(Cr_{1-x}Ga_x)_2O_4$ ($x = 0$, 0.05, 0.10, 0.15, and 0.20) samples under ZFC and FC conditions. The inset shows the inverse magnetic susceptibility and the fitting of the Curie–Weiss law for the undoped sample $MgCr_2O_4$ compound.

Furthermore, the ZFC and FC $\chi(T)$ curves of Ga-doped samples bifurcate below $T_N$, with the downturn in the ZFC branch and the upturn in the FC branch, implying the emergence of spin-glass behaviors [44,45]. The inset in Figure 3 displays the inverse magnetic susceptibility curve and its Curie–Weiss fit for $MgCr_2O_4$. The data in the high-temperature range (200 K $\leq$ T $\leq$ 300 K) were fitted using the Curie–Weiss law, $\chi = C/(T - \theta_{CW})$, where $\chi$ denotes the magnetic susceptibility, $C$ represents the Curie constant, and $\theta_{CW}$ stands for the Curie–Weiss temperature, as shown in Figure 4. The fitted Weiss temperature $|\theta_{CW}|$ for $MgCr_2O_4$ is $-516$ K, which deviates significantly from previously reported values [25,30,46]. This discrepancy may be attributed to the modified synthesis process

in which a 1% reduction in the $Cr_2O_3$ precursor mass leading to a pure phase $MgCr_2O_4$ product. Enhanced phase purity likely strengthens intrinsic antiferromagnetic interactions, thereby increasing the magnitude of $\theta_{CW}$.

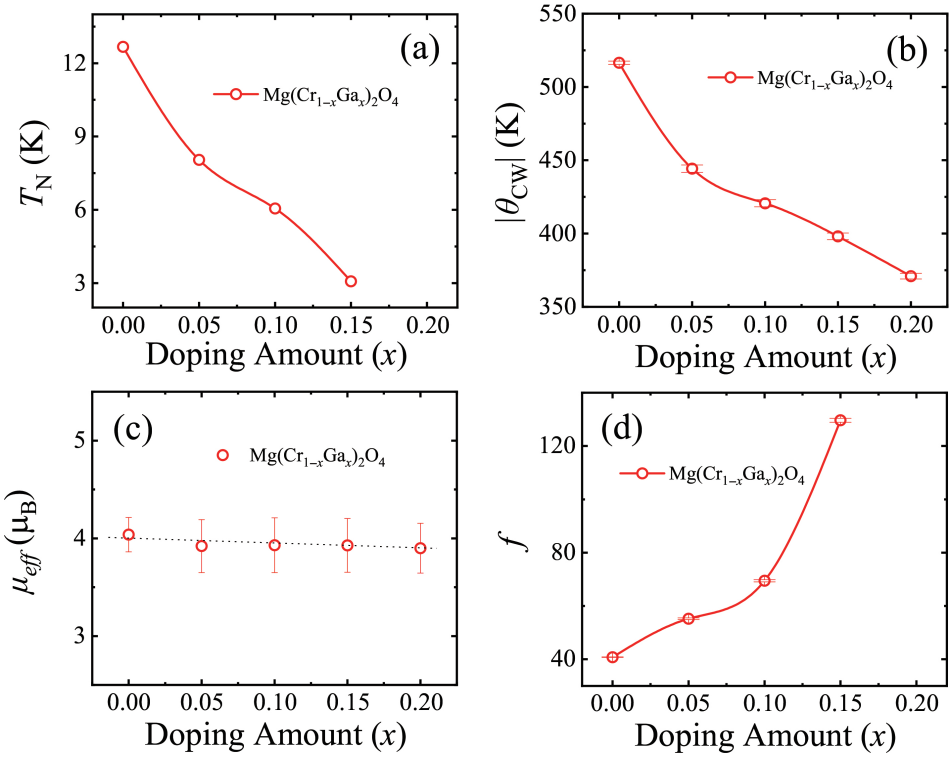



**Figure 4.** Extracted results from the DC magnetic susceptibilities for $Mg(Cr_{1-x}Ga_x)_2O_4$ ($x = 0$, 0.05, 0.10, 0.15, and 0.20). Néel temperature $T_N$ (**a**), Curie–Weiss temperature $|\theta_{CW}|$ (**b**), effective magnetic moment ($\mu_{eff}$) (**c**), and the frustration factor ($f = |\theta_{CW}|/T_N$) (**d**) vs. $Ga^{3+}$ doping level. Detailed data can be found in Table A3 of the Appendix A.

With increasing $Ga^{3+}$ doping, $\theta_{CW}$ decreases monotonically [Figure 4b], indicating suppression of antiferromagnetic interactions. The effective magnetic moment per $Cr^{3+}$ ion ($\mu_{eff}$) remains essentially unchanged upon doping [Figure 4c]. The magnetic frustration parameter, defined as $f = |\theta_{CW}|/T_N$, further increases with Ga doping [Figure 4d], indicating enhanced magnetic frustration. This effect may arise from the disruption of lattice periodicity due to partial substitution of magnetic B-site ions, leading to the formation of spatially heterogeneous [$Cr_3Ga_1$] tetrahedral clusters. The competition between Cr–Cr superexchange interactions in undoped regions and Cr–Ga–Cr exchange pathways at dopant boundaries introduces additional magnetic frustration within the system.

The XRD refinement confirms that $Ga^{3+}$ ions occupy both A and B-sites, where A-sites are typically non-magnetic, and $Cr^{3+}$ ions at magnetic B-sites are diluted. This substitution leads to structural distortions in the $Mg(Cr_{1-x}Ga_x)_2O_4$ lattice. Figure 3 illustrates the evolution of magnetic phases with increasing Ga doping. Intermediate doping levels ($x = 0.05$–$0.10$) display spin-glass-like behavior, evidenced by the bifurcation between ZFC and FC curves. At higher doping levels ($x \geq 0.15$), the system gradually transitions into a paramagnetic state, evidenced by the disappearance of the ZFC–FC splitting.

In $ZnCr_2O_4$, $Ga^{3+}$ ions predominantly substitute for $Cr^{3+}$ ions at the B-site, with minimal incorporation into the A-site ($Zn^{2+}$), resulting in a relatively well-defined doping process [37]. This "magnetic site dilution" disrupts the $Cr^{3+}$-based magnetic tetrahedral network, progressively weakening the antiferromagnetic order and inducing a spin-glass state. In contrast, in $MgCr_2O_4$, due to the closer ionic radii of $Mg^{2+}$ and $Ga^{3+}$, $Ga^{3+}$ ions not only occupy the B-site $Cr^{3+}$ positions but also partially substitute for A-site $Mg^{2+}$,

leading to A/B-site mixing and cation disorder. This more complex site occupancy results in an anomalous lattice contraction and introduces stronger perturbations to the magnetic structure, thereby suppressing the antiferromagnetic order at lower doping levels and giving rise to more pronounced spin-glass behavior.

According to Ch. Kant et al. [42], both nearest-neighbor ($J_1$) and next-nearest-neighbor ($J_2$) magnetic exchange interactions are present among B-site $Cr^{3+}$ ions, with $J_2$ generally weaker than $J_1$. Their theoretical model indicates that the $J_2$ is antiferromagnet in $MgCr_2O_4$ and $ZnCr_2O_4$ while transitioning to ferromagnetic in highly structurally distorted analogs like $CdCr_2O_4$. These findings are corroborated by previous reports on $Zn(Cr_{1-x}Ga_x)_2O_4$ [37]. In $Mg(Cr_{1-x}Ga_x)_2O_4$, the structural distortion may be strong enough to trigger the change of the magnetic interactions. A ferromagnetic $J_2$ might be induced with the sample of $x = 0.15$, leading to the observed ferromagnetic behavior in this system.

### 3.2. $MgCr_2O_4$ Doped with Cd

X-ray powder diffraction experiments were conducted at room temperature on polycrystalline $Mg(Cr_{1-x}Cd_x)_2O_4$($x$ = 0, 0.05, 0.10, 0.15, and 0.20). As shown in Figure 5, the diffraction patterns confirm phase purity for all samples, with no detectable secondary phases. Rietveld refinement of the X-ray data reveals crystallization in the cubic spinel structure with space group $Fd\bar{3}m$ (No. 227). As shown in Figure 5a, the normalized X-ray diffraction patterns suggest a systematic decrease in the intensity of the (111) reflection with increasing Cd content, indicating the successful $Cd^{2+}$ substitution into the $MgCr_2O_4$ lattice.

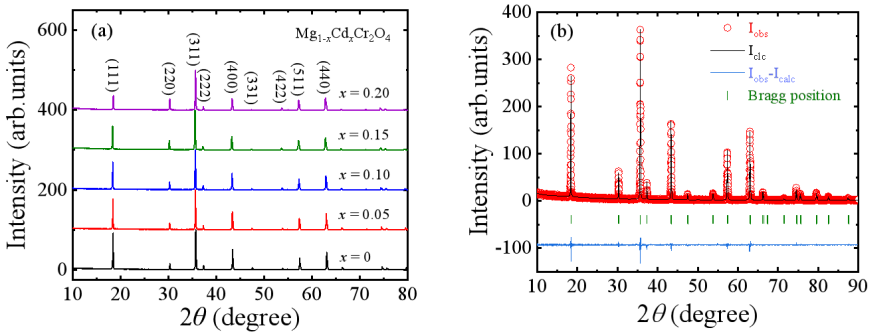



**Figure 5.** (**a**) The XRD patterns of the $Mg_{1-x}Cd_xCr_2O_4$ ($x$ = 0, 0.05, 0.10, 0.15, and 0.20) series of samples and (**b**) the Rietveld refinement plots for $Mg_{1-x}Cd_xCr_2O_4$ ($x$ = 0.05).

Figure 5b presents a representative X-ray Rietveld refinement profile of $Mg_{1-x}Cd_xCr_2O_4$ for $x = 0.05$. The full refinement results for all Cd-doped samples are summarized in Figure 6. Figure 6a shows good agreement between the actual Cd concentrations and the nominal doping levels, confirming the accuracy of the composition control. Figure 6d displays the average ionic radius at the A-site, derived from the actual Cd doping levels. The radius increases linearly with doping, indicating effective substitution of $Mg^{2+}$ by the larger $Cd^{2+}$ ions. There is also an implication that no Cd ions take the site of Cr. Figure 6b,c present the refined lattice parameter $a$, along with the interatomic distances $d_1$ (Cr–Cr) and $d_2$ (Mg–Mg), respectively. All structural parameters increase monotonically with Cd content, indicating that Cd doping leads to lattice expansion and structural distortion in the $MgCr_2O_4$ system.

Figure 7 displays the ZFC and FC susceptibility curves of $Mg_{1-x}Cd_xCr_2O_4$ ($x = 0$, 0.05, 0.10, 0.15, and 0.20), measured under an external magnetic field of 0.2 T. As temperature decreases, larger bifurcation between ZFC and FC susceptibility curves were observed. A distinct bifurcation emerges at the spin-glass transition temperature ($T_f$), which becomes more pronounced with higher Cd content. As shown in Figure 8a, $T_N$ decreases from

12.6 K to 6 K with increasing Cd doping. Figure 8b shows that the Weiss temperature ($\theta_{CW}$), obtained from Curie–Weiss fitting, decreases with increasing $x$ in the range $0 \leq x \leq 0.125$ but slightly increases for $0.125 \leq x \leq 0.20$. This suggests that the suppression of antiferromagnetic interactions saturates near $x = 0.125$. Figure 8c shows that the frustration factor $f = |\theta_{CW}|/T_N$ reaches a minimum at $x = 0.125$, indicating maximal suppression of magnetic frustration. The effective magnetic moment ($\mu_{eff}$) remains nearly constant across all doping levels. Previous investigations on Cd-doped $ZnCr_2O_4$ have demonstrated that the introduction of $Cd^{2+}$ ions not only reduces the $T_N$ but also effectively suppresses long-range antiferromagnetic ordering, leading to a spin-glass-like state [38]. Similarly, in the present study on $MgCr_2O_4$, $Cd^{2+}$ doping exhibits a comparable trend, with $T_N$ decreasing and AFM order gradually replaced by spin-glass behavior. This consistency across both Zn and Mg based spinels underscores the crucial role of A-site non-magnetic ion substitution in disrupting magnetic interactions and tuning the magnetic ground state in geometrically frustrated spinel systems.

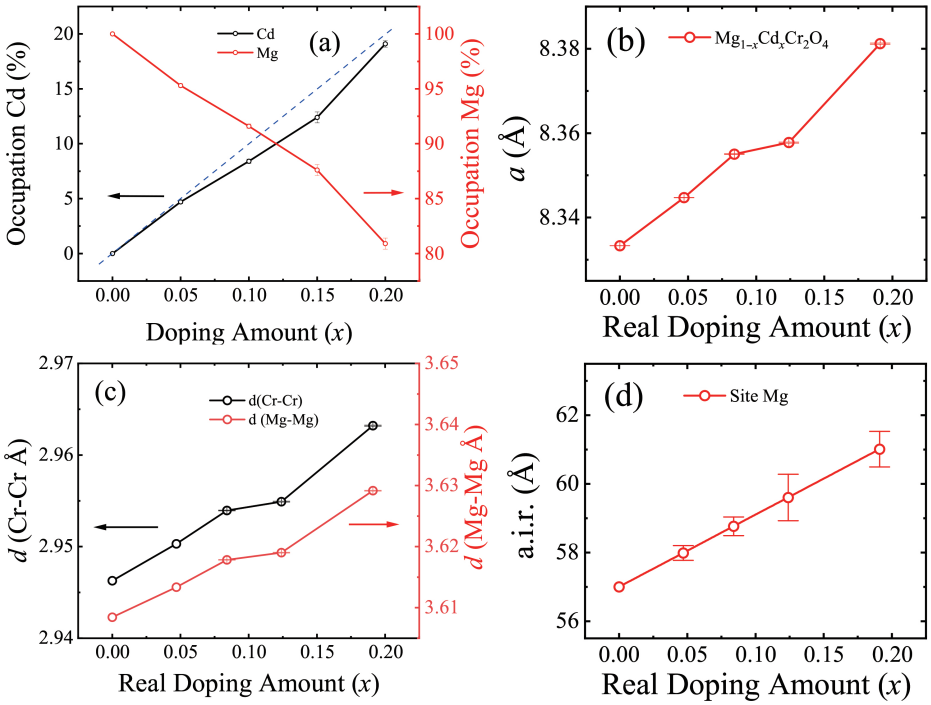



**Figure 6.** (**a**) The changes in the occupancy of $Mg^{2+}$ and $Cd^{2+}$ ions at the Mg-site, (**b**) the variation of the lattice constant, (**c**) the variations of Cr-Cr and Mg-Mg bond lengths, and (**d**) the variation in the average ionic radii (a.i.r.) at the Mg site. Detailed data can be found in Table A4 of the Appendix A.

Unlike Ga doping, XRD refinement confirms that $Cd^{2+}$ substitutes exclusively at the A-site and does not affect the magnetic $Cr^{3+}$ ions at the B-site. The $\chi(T)$ data reveal that even at $x = 0.05$, Cd doping induces a magnetic transition from antiferromagnetic to spin-glass behavior, which persists even at high doping concentrations, similar to the previously reported behavior of $Zn_{1-x}Cd_xCr_2O_4$ [38]. This early transition is likely driven by the large ionic radius mismatch (21 pm) between $Cd^{2+}$ and $Mg^{2+}$, compared to the smaller mismatches between $Ga^{3+}$ and $Cr^{3+}$ (0.5 pm) or $Mg^{2+}$ (10 pm). The pronounced ionic size mismatch induces lattice distortions, which mediate the antiferromagnetic-to-spin-glass crossover at dilute doping concentrations. In studies on $ZnCr_2O_4$ [38], $Ga^{3+}$ doping has been found to dilute the $Cr^{3+}$ sublattice, introducing site disorder that suppresses the long-range antiferromagnetic ordering. In contrast, $Cd^{2+}$ doping induces bond disorder by randomly modifying Cr–Cr exchange interactions, thereby promoting a transition into a spin-glass state. Given the high degree of similarity between $MgCr_2O_4$ and $ZnCr_2O_4$, it is

reasonable to extend this interpretation to the $MgCr_2O_4$ system. Therefore, $Cd^{2+}$ doping in $MgCr_2O_4$ effectively suppresses magnetic ordering while preserving a corner sharing tetrahedral lattice composed entirely of magnetic $Cr^{3+}$ ions, making it an ideal candidate for investigating the origin of resonance magnetic excitations in $MgCr_2O_4$.

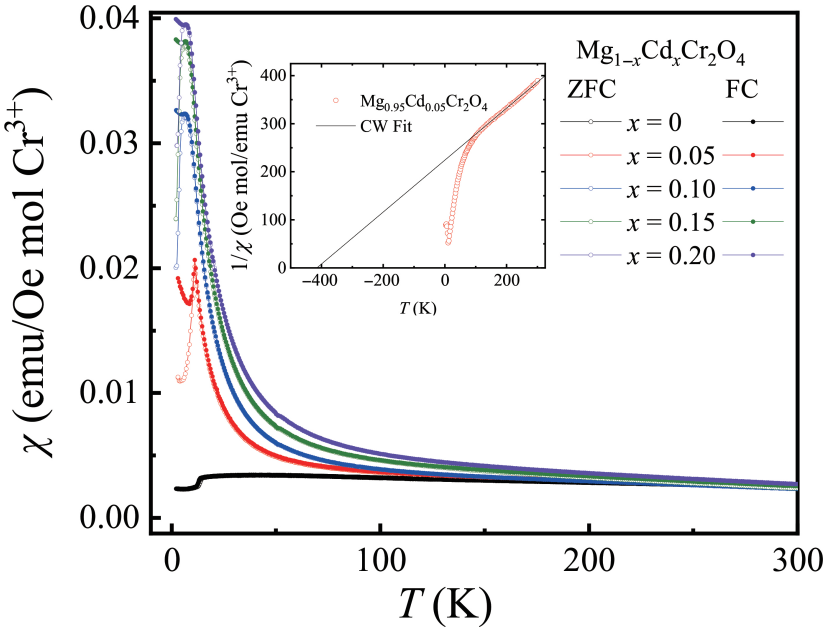



**Figure 7.** Temperature-dependent ZFC and FC DC magnetic susceptibility $\chi(T)$ curves for $Mg_{1-x}Cd_xCr_2O_4$ ($x$ = 0, 0.05, 0.10, 0.15, and 0.20) measured under an applied magnetic field of 0.2 T. The inset displays the inverse susceptibility $\chi^{-1}(T)$ for $Mg_{0.95}Cd_{0.05}Cr_2O_4$ with Curie–Weiss fitting. As $Cd^{2+}$ doping increases, the $T_N$ systematically shifts to lower temperatures, indicating a progressive suppression of AFM interactions. The increased bifurcation between ZFC and FC curves at higher doping levels suggests the emergence of spin-glass-like behavior.

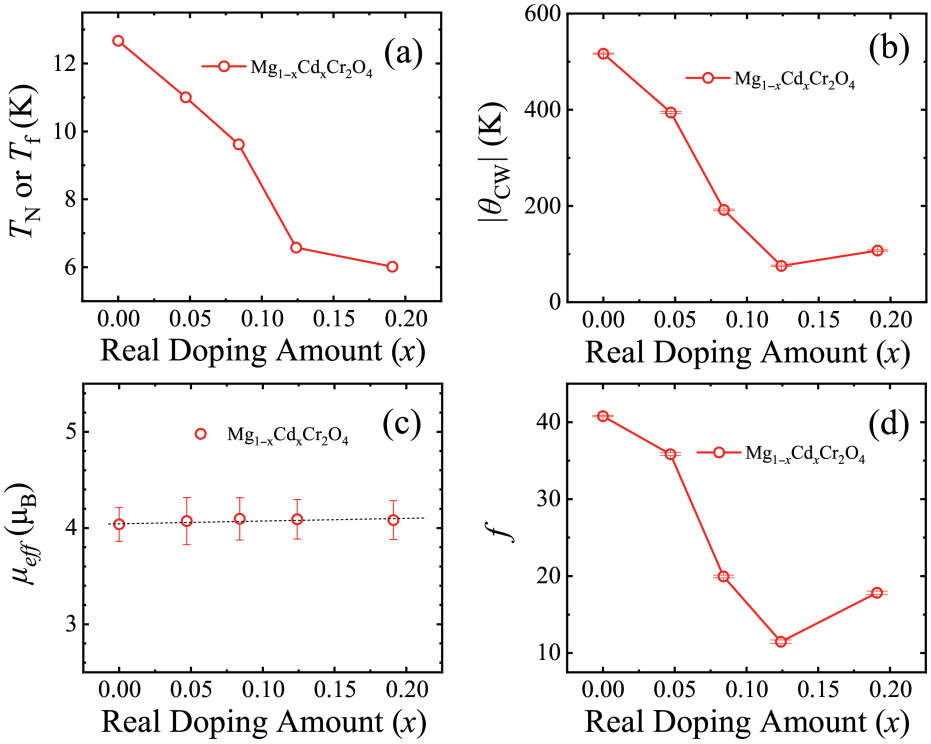



**Figure 8.** (**a**) Magnetic transition temperature $T_N$, (**b**) Weiss temperature $\theta_{CW}$, (**c**) effective magnetic moment $\mu_{eff}$, and (**d**) magnetic frustration coefficient $f$ as a function of $Cd^{2+}$ doping concentration in $Mg_{1-x}Cd_xCr_2O_4$. Detailed data can be found in Table A5 of the Appendix A.

## 4. Conclusions

In summary, we successfully synthesized a series of Ga and Cd-doped $MgCr_2O_4$ spinel oxides via solid-state reaction. Doping with $Ga^{3+}$ or $Cd^{2+}$ ions preserved the cubic spinel structure of the parent $MgCr_2O_4$ system. Structural refinement of the XRD data reveals an anomalous decrease in the lattice constant of $MgCr_2O_4$ with increasing $Ga^{3+}$ doping concentration. This behavior is attributed to cation site disorder and structural distortions induced by doping. Furthermore, NPD refinement performed on the $x = 0.20$ sample confirms that $Ga^{3+}$ ions not only substitute for $Cr^{3+}$ at the B-site but also partially occupy the A-site positions originally held by $Mg^{2+}$, resulting in a complex composition with the chemical formula $(Mg_{1-x}Ga_x)(Cr_{1-y}Ga_y)_2O_4$. This provides direct experimental evidence for the dual-site occupation of $Ga^{3+}$ in the $MgCr_2O_4$ lattice. Magnetic susceptibility measurements show that $Ga^{3+}$ doping progressively transforms the system from an antiferromagnetic state into a spin-glass-like state in the $x = 0$–$0.10$ range and completely suppresses the antiferromagnetic transition at $x = 0.20$, likely due to magnetic site dilution by $Ga^{3+}$. In contrast, $Cd^{2+}$ doping leads to lattice expansion, and Rietveld refinements confirm that $Cd^{2+}$ exclusively substitutes for $Mg^{2+}$ at the A-sites. Magnetic measurements demonstrate that even low levels of $Cd^{2+}$ doping induce spin-glass-like behavior, with complete suppression of the antiferromagnetic transition at 10% doping level. This is attributed to lattice distortions caused by the large ionic radius of $Cd^{2+}$, which disrupt magnetic exchange paths and destabilize long-range order. Accordingly, considering both the preserved $Cr^{3+}$ magnetic tetrahedral lattice and the enhanced suppression of magnetic order, 10% Cd-doped $MgCr_2O_4$ serves as an ideal material platform for future inelastic neutron scattering studies aimed at isolating and understanding the origin of resonant magnetic excitations. This work provides both sample materials and preliminary research foundations for understanding the origin of the resonant magnetic excitation modes in $MgCr_2O_4$.

**Author Contributions:** Conceptualization, E.F. and Z.H.; investigation, F.Z., D.C., W.Z., and Z.F.; methodology, F.Z., Z.H., D.C., X.W., and Z.F.; resources, H.G., L.W., W.L., X.L., and L.H.; writing—original draft preparation, F.Z., Z.H., X.W., and P.Z.; writing—review and editing, E.F. and Y.Z.; funding acquisition, E.F. and Z.H. All authors have read and agreed to the published version of the manuscript.

**Funding:** The project was supported by National Natural Science Foundation of China, No. 12375298, the Large Scientific Facility Open Subject of Songshan Lake, Dongguan, Guangdong, KFKT2022B05, and the China Postdoctoral Science Foundation under Grant No. 2024M751754.

**Data Availability Statement:** The original contributions presented in this study are included in the article. Further inquiries can be directed to the corresponding authors.

**Acknowledgments:** This research used resources at the China Spallation Neutron Source (CSNS). We thank Guang Wang for supporting the laboratory work. We also acknowledge OpenAI for providing access to the GPT-4 language model, which was utilized for language refinement of the manuscript.

**Conflicts of Interest:** The authors declare no competing financial interests. Correspondence and requests for materials should be addressed to Erxi Feng.

## Appendix A

**Table A1.** Wyckoff positions and atomic positions of each atom of $Mg(Cr_{1-x}Ga_x)_2O_4$ ($x$ = 0.20) obtained by neutron powder diffraction.

| Atom | Wyckoff Position | x | y | z |
|---|---|---|---|---|
| O | 32e | 0.26004 | 0.26004 | 0.26004 |
| Cr | 16d | 0.50000 | 0.50000 | 0.50000 |
| Ga(1) | 16d | 0.50000 | 0.50000 | 0.50000 |
| Mg | 8a | 0.12500 | 0.12500 | 0.12500 |
| Ga(2) | 8a | 0.12500 | 0.12500 | 0.12500 |

**Table A2.** Refined lattice constant $a$, site occupancies of Cr and Ga at the B-sites, site occupancies of Mg and Ga at the A-sites, and $Cr-Cr$ and $Mg-Mg$ bond lengths for the $Mg(Cr_{1-x}Ga_x)_2O_4$ series.

| $x$ | $a$ (Å) | $d_{Mg-Mg}$ (Å) | $d_{Cr-Cr}$ (Å) | B-Site Occupancy (%) | | A-Site Occupancy (%) | |
|---|---|---|---|---|---|---|---|
| | | | | Cr | Ga | Mg | Ga |
| 0 | 8.33333 (3) | 3.60844 (0) | 2.94628 (0) | 100.0 (1) | 0 | 100.0 (1) | 0 |
| 0.05 | 8.33293 (17) | 3.60744 (8) | 2.94546 (7) | 95.7 (1) | 4.3 (1) | 98.6 (1) | 1.4 (1) |
| 0.10 | 8.33111 (21) | 3.60678 (9) | 2.94492 (8) | 92.9 (1) | 7.1 (1) | 94.2 (1) | 5.8 (1) |
| 0.15 | 8.32714 (19) | 3.60546 (9) | 2.94385 (7) | 92.8 (1) | 7.2 (1) | 84.4 (1) | 15.6 (1) |
| 0.20 | 8.32183 (13) | 3.60275 (6) | 2.94163 (5) | 92.3 (2) | 7.7 (2) | 75.4 (2) | 24.6 (2) |

**Table A3.** Magnetic phase transition temperature $T_N$, Weiss temperature $\theta_{CW}$, effective magnetic moment $\mu_{eff}$, and frustration factor $f$ for $Mg(Cr_{1-x}Ga_x)_2O_4$.

| $Mg(Cr_{1-x}Ga_x)_2O_4$ | $T_N$ (K) | $\theta_{CW}$ (K) | $\mu_{eff}$ ($\mu_B$) | $f$ |
|---|---|---|---|---|
| 0 | 12.6 | −516.498 (11) | 4.04 (18) | 40.77 (9) |
| 0.05 | 8.0 | −444.311 (25) | 3.92 (27) | 55.23 (31) |
| 0.10 | 6.1 | −420.684 (25) | 3.93 (28) | 69.46 (41) |
| 0.15 | 3.1 | −398.092 (23) | 3.93 (27) | 129.67 (75) |
| 0.20 | <2.0 | −370.944 (19) | 3.90 (25) | >123.49 (64) |

**Table A4.** Refined lattice constant $a$, site occupancies of Mg and Cd at the A-sites, and $Cr-Cr$ and $Mg-Mg$ bond lengths for the $Mg_{1-x}Cd_xCr_2O_4$ series.

| $x$ | $a$ (Å) | $d_{Cr-Cr}$ (Å) | $d_{Mg-Mg}$ (Å) | A-Site Occupancy (%) | |
|---|---|---|---|---|---|
| | | | | Mg | Cd |
| 0 | 8.33333 (3) | 2.94628 (0) | 3.60844 (0) | 100.0 (1) | 0 |
| 0.05 | 8.34472 (4) | 2.9503 (0) | 3.61337 (0) | 95.3 (2) | 4.7 (2) |
| 0.10 | 8.35502 (9) | 2.95395 (4) | 3.61783 (4) | 91.6 (2) | 8.4 (2) |
| 0.15 | 8.35776 (13) | 2.95491 (5) | 3.61902 (6) | 87.6 (5) | 12.4 (5) |
| 0.20 | 8.38121 (14) | 2.96321 (6) | 3.62917 (7) | 80.9 (5) | 19.1 (3) |

**Table A5.** Magnetic phase transition temperature $T_N$, Weiss temperature $\theta_{CW}$, effective magnetic moment $\mu_{eff}$, and frustration factor $f$ for $Mg_{1-x}Cd_xCr_2O_4$.

| $Mg_{1-x}Cd_xCr_2O_4$ | $T_N$ (K) | $\theta_{CW}$ (K) | $\mu_{eff}$ ($\mu_B$) | $f$ |
|---|---|---|---|---|
| 0 | 12.667 | −516.5 (11) | 4.04 (18) | 40.77 (9) |
| 0.05 | 11.004 | −394.3 (19) | 4.07 (24) | 35.84 (17) |
| 0.10 | 9.616 | −191.8 (17) | 4.10 (22) | 19.95 (17) |
| 0.15 | 6.579 | −75.4 (15) | 4.09 (21) | 11.46 (23) |
| 0.20 | 6.015 | −107.2 (13) | 3.08 (20) | 17.83 (21) |

## References

1. Balents, L. Spin liquids in frustrated magnets. *Nature* **2010**, *464*, 199–208. [CrossRef] [PubMed]
2. Moessner, R.; Ramirez, A.P. Geometrical frustration. *Phys. Today* **2006**, *59*, 24–29. [CrossRef]

3. Rao, X.; Hussain, G.; Huang, Q.; Chu, W.J.; Li, N.; Zhao, X.; Dun, Z.; Choi, E.S.; Asaba, T.; Chen, L.; et al. Survival of itinerant excitations and quantum spin state transitions in $YbMgGaO_4$ with chemical disorder. *Nat. Commun.* **2021**, *12*, 4949. [CrossRef]
4. Helton, J.S.; Matan, K.; Shores, M.P.; Nytko, E.A.; Bartlett, B.M.; Qiu, Y.; Nocera, D.G.; Lee, Y.S. Dynamic scaling in the susceptibility of the spin-1/2 kagome lattice antiferromagnet Herbertsmithite. *Phys. Rev. Lett.* **2010**, *104*, 147201. [CrossRef]
5. Khuntia, P.; Velazquez, M.; Barthélemy, Q.; Bert, F.; Kermarrec, E.; Legros, A.; Bernu, B.; Messio, L.; Zorko, A.; Mendels, P. Gapless ground state in the archetypal quantum kagome antiferromagnet $ZnCu_3(OH)_6Cl_2$. *Nat. Phys.* **2020**, *16*, 469–474. [CrossRef]
6. Han, T.H.; Helton, J.S.; Chu, S.; Nocera, D.G.; Rodriguez-Rivera, J.A.; Broholm, C.; Lee, Y.S. Fractionalized excitations in the spin-liquid state of a kagome-lattice antiferromagnet. *Nature* **2012**, *492*, 406–410. [CrossRef]
7. Schweika, W.; Valldor, M.; Lemmens, P. Approaching the ground state of the kagomé antiferromagnet. *Phys. Rev. Lett.* **2007**, *98*, 067201. [CrossRef]
8. Stewart, J.R.; Ehlers, G.; Mutka, H.; Fouquet, P.; Payen, C.; Lortz, R. Spin dynamics, short-range order, and spin freezing in $Y_{0.5}Ca_{0.5}BaCo_4O_7$. *Phys. Rev. B—Condensed Matter Mater. Phys.* **2011**, *83*, 024405. [CrossRef]
9. Okamoto, Y.; Nohara, M.; Aruga-Katori, H.; Takagi, H. Spin-liquid state in the S = 1/2 hyperkagome antiferromagnet $Na_4Ir_3O_8$. *Phys. Rev. Lett.* **2007**, *99*, 137207. [CrossRef] [PubMed]
10. Gardner, J.S.; Gingras, M.J.P.; Greedan, J.E. Magnetic pyrochlore oxides. *Rev. Mod. Phys.* **2010**, *82*, 53–107. [CrossRef]
11. Siddharthan, R.; Shastry, B.S.; Ramirez, A.P.; Hayashi, A.; Cava, R.J.; Rosenkranz, S. Ising pyrochlore magnets: Low-temperature properties, "ice rules," and beyond. *Phys. Rev. Lett.* **1999**, *83*, 1854. [CrossRef]
12. Gingras, M.J.P.; McClarty, P.A. Quantum spin ice: A search for gapless quantum spin liquids in pyrochlore magnets. *Rep. Prog. Phys.* **2014**, *77*, 056501. [CrossRef]
13. Bramwell, S.T.; Gingras, M.J.P. Spin ice state in frustrated magnetic pyrochlore materials. *Science* **2001**, *294*, 1495–1501. [CrossRef] [PubMed]
14. Matsuhira, K.; Hinatsu, Y.; Tenya, K.; Amitsuka, H.; Sakakibara, T. Low-temperature magnetic properties of pyrochlore stannates. *J. Phys. Soc. Jpn.* **2002**, *71*, 1576–1582. [CrossRef]
15. Shapiro, M.C.; Riggs, S.C.; Stone, M.B.; de la Cruz, C.R.; Chi, S.; Podlesnyak, A.A.; Fisher, I.R. Structure and magnetic properties of the pyrochlore iridate $Y_2Ir_2O_7$. *Phys. Rev. B* **2012**, *85*, 214434. [CrossRef]
16. Xu, J.; Anand, V.K.; Bera, A.K.; Frontzek, M.; Abernathy, D.L.; Casati, N.; Siemensmeyer, K.; Lake, B. Magnetic structure and crystal-field states of the pyrochlore antiferromagnet $Nd_2Zr_2O_7$. *Phys. Rev. B* **2015**, *92*, 224430. [CrossRef]
17. Das, D.; Ghosh, S. Density functional theory based comparative study of electronic structures and magnetic properties of spinel $ACr_2O_4$ (A = Mn, Fe, Co, Ni) compounds. *J. Phys. D Appl. Phys.* **2015**, *48*, 425001. [CrossRef]
18. Ali, A.; Singh, Y. A magnetocaloric study on the series of 3d-metal chromites $ACr_2O_4$ (A = Mn, Fe, Co, Ni, Cu and Zn). *J. Magn. Magn. Mater.* **2020**, *499*, 166253. [CrossRef]
19. Kassem, M.A.; El-Fadl, A.A.; Nashaat, A.M.; Nakamura, H. Structure, optical and varying magnetic properties of insulating $MCr_2O_4$ (M = Co, Zn, Mg and Cd) nanospinels. *J. Alloys Compd.* **2019**, *790*, 853–862. [CrossRef]
20. Moureen, C.K.; Stephanie, L.M.; Lucy, E.D.; Ram, S.; Matthew, R.S.; Daniel, P.S.; Katharine, P.; Joan, S. Structural ground states of $(A,A')Cr_2O_4$ (A = Mg, Zn; A′ = Co, Cu) spinel solid solutions: Spin-Jahn-Teller and Jahn-Teller effects. *Phys. Rev. B* **2014**, *89*, 174410.
21. Ohgushi, K.; Okimoto, Y.; Ogasawara, T.; Miyasaka, S.; Tokura, Y. Magnetic, optical, and magnetooptical properties of spinel-type $ACr_2X_4$ (A = Mn, Fe, Co, Cu, Zn, Cd; X = O, S, Se). *J. Phys. Soc. Jpn.* **2008**, *77*, 034713. [CrossRef]
22. Lau, G.C.; Ueland, B.G.; Freitas, R.S.; Dahlberg, M.L.; Schiffer, P.; Cava, R.J. Magnetic characterization of the sawtooth-lattice olivines $ZnL_2S_4$ (L = Er, Tm, Yb). *Phys. Rev. B* **2006**, *73*, 012413. [CrossRef]
23. Zhandun, V.S. The magnetic, electronic, optical, and structural properties of the $AB_2O_4$ (A = Mn, Fe, Co; B = Al, Ga, In) spinels: Ab initio study. *J. Magn. Magn. Mater.* **2021**, *533*, 168015. [CrossRef]
24. Ortega-San-Martin, L.; Williams, A.J.; Gordon, C.D.; Klemme, S.; Attfield, J.P. Low temperature neutron diffraction study of $MgCr_2O_4$ spinel. *J. Phys. Condens. Matter* **2008**, *20*, 104238. [CrossRef]
25. Dutton, S.E.; Huang, Q.; Tchernyshyov, O.; Broholm, C.L.; Cava, R.J. Sensitivity of the magnetic properties of the $ZnCr_2O_4$ and $MgCr_2O_4$ spinels to nonstoichiometry. *Phys. Rev. B* **2011**, *83*, 064407. [CrossRef]
26. Bai, X.; Paddison, J.A.M.; Kapit, E.; Koohpayeh, S.M.; Wen, J.-J.; Dutton, S.E.; Savici, A.T.; Kolesnikov, A.I.; Granroth, G.E.; Broholm, C.L.; et al. Magnetic excitations of the classical spin liquid $MgCr_2O_4$. *Phys. Rev. Lett.* **2019**, *122*, 097201. [CrossRef] [PubMed]
27. Zhou, H.D.; Zhao, Z.Y.; Sun, X.F.; Suarez, M.N.; Rivas-Murias, B.; Tsurkan, V.; Deisenhofer, J.; Zapf, V.S.; Rivadulla, F. Low-temperature spin excitations in frustrated $ZnCr_2O_4$ probed by high-field thermal conductivity. *Phys. Rev. B* **2013**, *87*, 174436. [CrossRef]
28. Matsuda, M.; Ueda, H.; Kikkawa, A.; Tanaka, Y.; Katsumata, K.; Narumi, Y.; Inami, T.; Ueda, Y.; Lee, S.-H. Spin–lattice instability to a fractional magnetization state in the spinel $HgCr_2O_4$. *Nat. Phys.* **2007**, *3*, 397–400. [CrossRef]

29. Ueda, H.; Mitamura, H.; Goto, T.; Ueda, Y. Field-induced metamagnetic transitions in S = 3/2 Heisenberg antiferromagnets $MCr_2O_4$. *Prog. Theor. Phys. Suppl.* **2005**, *159*, 256–259. [CrossRef]
30. Rudolf, T.; Kant, C.; Mayr, F.; Hemberger, J.; Tsurkan, V.; Loidl, A. Spin-phonon coupling in antiferromagnetic chromium spinels. *New J. Phys.* **2007**, *9*, 76. [CrossRef]
31. Shaked, H.; Hastings, J.M.; Corliss, L.M. Magnetic structure of magnesium chromite. *Phys. Rev. B* **1970**, *1*, 3116. [CrossRef]
32. Suzuki, H.; Tsunoda, Y. Spinel-type frustrated system $MgCr_2O_4$ studied by neutron scattering and magnetization measurements. *J. Phys. Chem. Solids* **2007**, *68*, 2060–2063. [CrossRef]
33. Gao, S.; Guratinder, K.; Stuhr, U.; White, J.S.; Mansson, M.; Roessli, B.; Fennell, T.; Tsurkan, V.; Loidl, A.; Hatnean, M.C.; et al. Manifolds of magnetic ordered states; and excitations in the almost Heisenberg pyrochlore antiferromagnet $MgCr_2O_4$. *Phys. Rev. B* **2018**, *97*, 134430. [CrossRef]
34. Tomiyasu, K.; Suzuki, H.; Toki, M.; Itoh, S.; Matsuura, M.; Aso, N.; Yamada, K. Molecular spin resonance in the geometrically frustrated magnet $MgCr_2O_4$ by inelastic neutron scattering. *Phys. Rev. Lett.* **2008**, *101*, 177401. [CrossRef]
35. Yong, W.; Botis, S.; Shieh, S.R.; Shi, W.; Withers, A.C. Pressure-induced phase transition study of magnesiochromite ($MgCr_2O_4$) by Raman spectroscopy and X-ray diffraction. *Phys. Earth Planet. Inter.* **2012**, *196*, 75–82. [CrossRef]
36. Lee, S.-H.; Ratcliff, W., II; Huang, Q.; Kim, T.H.; Cheong, S.-W. Néel to spin-glass-like phase transition versus dilution in geometrically frustrated $ZnCr_{2-2x}Ga_{2x}O_4$. *Phys. Rev. B* **2008**, *77*, 014405. [CrossRef]
37. Yu, J.; Wang, L.; Ying, Y.; Zheng, J.; Li, W.; Qiao, L.; Cai, W.; Li, J.; Zhang, L.; Che, S. Magnetic Exchange Interactions in Geometrically Frustrated Antiferromagnet of $ZnCr_{2-x}Ga_xO_4$. *J. Supercond. Nov. Magn.* **2019**, *32*, 1095–1098. [CrossRef]
38. Martinho, H.; Moreno, N.O.; Sanjurjo, J.A.; Rettori, C.; Âa-Adeva, A.J.G.; Huber, D.L.; Oseroff, S.B.; Ratcliff, W., II; Cheong, S.-W.; Pagliuso, P.G.; et al. Magnetic properties of the frustrated antiferromagnetic spinel $ZnCr_2O_4$ and the spin-glass $Zn_{1-x}Cd_xCr_2O_4$ (x = 0.05, 0.10). *Phys. Rev. B* **2001**, *64*, 024408. [CrossRef]
39. Ohta, H.; Okubo, S.; Kikuchi, H.; Ono, S. Millimetre-wave ESR (electron-spin resonance) measurements of frustrated system $ZnCr_{2x}Ga_{2-2x}O_4$. *Can. J. Phys.* **2001**, *79*, 1387–1391. [CrossRef]
40. Sears, V.F. Neutron scattering lengths and cross sections. *Neutron News* **1992**, *3*, 26–37. [CrossRef]
41. Shannon, R.D. Revised effective ionic radii and systematic studies of interatomic distances in halides and chalcogenides. *Found. Crystallogr.* **1976**, *32*, 751–767. [CrossRef]
42. Kant, C.; Deisenhofer, J.; Tsurkan, V.; Loidl, A. Magnetic susceptibility of the frustrated spinels $ZnCr_2O_4$, $MgCr_2O_4$ and $CdCr_2O_4$. *J. Phys. Conf. Ser.* **2010**, *200*, 032032. [CrossRef]
43. Nassar, L.S.; Lane, H.; Haberl, B.; Graves-Brook, M.; Winn, B.; Koohpayeh, S.M.; Mourigal, M. Pressure control of magnetic order and excitations in the pyrochlore antiferromagnet $MgCr_2O_4$. *Phys. Rev. B* **2024**, *109*, 064415. [CrossRef]
44. Niu, X.; Liu, C.; Zong, B. Investigation on the microstructure and magnetic properties of $Mg(Ga_{2-X}Fe_x)O_4$ Spinel Ferrites. *J. Mater. Sci. Mater. Electron.* **2023**, *34*, 118. [CrossRef]
45. Das, A.; Ranaut, D.; Pal, P.; Pal, R.; Mandal, P.; Pal, A.N.; Moulick, S.; Das, M.; Topwal, D.; Mukherjee, K.; et al. Tuning of magnetic frustration and emergence of a magnetostructural transition in $Mn_{1-X}Cd_xCr_2O_4$. *Phys. Rev. B* **2023**, *108*, 064426. [CrossRef]
46. Koohpayeh, S.M.; Wen, J.-J.; Mourigal, M.; Dutton, S.E.; Cava, R.J.; Broholm, C.L.; McQueen, T.M. Optical floating zone crystal growth and magnetic properties of $MgCr_2O_4$. *J. Cryst. Growth* **2013**, *384*, 39–43. [CrossRef]


**Disclaimer/Publisher's Note:** The statements, opinions and data contained in all publications are solely those of the individual author(s) and contributor(s) and not of MDPI and/or the editor(s). MDPI and/or the editor(s) disclaim responsibility for any injury to people or property resulting from any ideas, methods, instructions or products referred to in the content.